RSC Advances

Organic solar cells based on bowl-shape small-molecules

Journal:	*RSC Advances*
Manuscript ID:	RA-ART-02-2015-002073.R2
Article Type:	Paper
Date Submitted by the Author:	19-Mar-2015
Complete List of Authors:	Molina, Agustin; IMDEA nanoscience, Gallego, Maria; IMDEA nanoscience, Echegoyen, Luis; University of Texas at El Paso, Department of Chemistry Perez, Emilio; Universidad Complutense de Madrid, Departamento de Quimica Organica Martin, Nazario; Facultad de Quimica, Departamento de Quimica Organica

Journal Name

RSCPublishing

ARTICLE

Organic solar cells based on bowl-shape small-molecules

Cite this: DOI: 10.1039/x0xx00000x

Received 00th January 2012,
Accepted 00th January 2012

DOI: 10.1039/x0xx00000x

www.rsc.org/

Agustín Molina-Ontoria,[a] María Gallego,[c] Luís Echegoyen,[a*] Emilio M. Pérez[b] and Nazario Martín[bc*]

Light absorption ability and morphology of the active components are two of the key factors that determine the energy conversion efficiency in organic solar cells (OSCs). Determining the relative importance of each of these aspects is decisive for the construction of more efficient OSCs. Here we introduce two π-extended derivatives of tetrathiafulvalene as electron donors for solution-processed small-molecule bulk-heterojunction solar cells. Both of them exhibit similar bowl-shape geometry, excellent electron-donor characteristics and moderately high association constants with fullerenes in solution (on the order of 10^4 M^{-1} for truxTTF and 10^3 M^{-1} for truxTTF-CO in several solvents at room temperature). The substitution of one dithiole ring in truxTTF-CO for a ketone results in an intramolecular push-pull effect, which enhances its light-haversting properties, with the onset of absorbance reaching 650 nm. The introduction of a third dithiole ring, results in a more pronounced concave shape in truxTTF, allowing a better self-assembly with fullerenes which in turn leads to a better control of the morphology. However, the light-absorption ability of truxTTF is limited to ca. 500 nm. We prepared bulk-heterojunction solar cells using phenyl-C_{60}-butyric acid methyl ester ($PC_{61}BM$) and $PC_{71}BM$ as electron-acceptors and bowl-shape truxTTF and truxTTF-CO as electron-donors. The devices prepared utilizing truxTTF performed significantly better (PCE up to 1.77% with $PC_{71}BM$ and 0.92% with $PC_{61}BM$) than truxTTF-CO counterpart (PCE up to 1.19% with $PC_{71}BM$ and 0.56% with $PC_{61}BM$).

Introduction

The photoactive layer of a bulk-heterojunction solar cell (BHJ) is composed of a blend of either a π-conjugated semiconductor polymer[1,2] or other small-molecule[3,4] as electron donors and a fullerene derivative or a small acceptor molecule, such as diketopyrrolopyrrole (DPP), perylenediimide (PDI) or fluoranthene-fused imide (FFI), as electron acceptors. An interpenetrating network at the nanometer scale (shorter than the exciton diffusion length ≈ 3-10 nm) of these two components is crucial for efficient exciton diffusion to the interfaces, followed by exciton dissociation into charges. Formation of percolating pathways for electrons and holes to be efficiently collected at the external electrodes is also needed to avoid undesired charge recombination processes. Therefore, control of the morphology of the active layer is a key issue in the preparation of BHJ solar cells, given its critical influence on the device performance.[5-11] There are several macroscopic methods to assist the control of the morphology, including the use of solvent additives[12-14] or solvent/thermal annealing.[15-22]

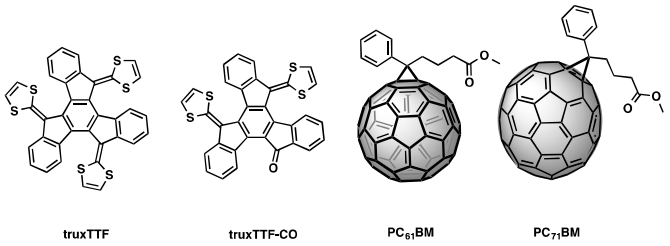

Figure 1. Chemical structures of bowl-shape electron donors truxTTF and truxTTF-CO and electron acceptors phenyl-C_{60}-butyric acid methyl ester ($PC_{61}BM$) and phenyl-C_{70}-butyric acid methyl ester ($PC_{71}BM$).

Moreover, a molecular approach has been used to control the phase segregation, for instance, by self-assembling fullerene derivatives,[23,24] by using the side chains of the polymers to accommodate the acceptor moieties[25-27] or by means of hydrogen-bonding.[28-31] However, in these macroscopic and molecular approaches, the donor and acceptor moieties act individually, since there are no specific interactions between

them. On the other hand, a supramolecular approach in which both components interact through their complementary shapes has been reported only recently.[32-34] Coronene derivatives (donor) were found to form supramolecular complexes with $PC_{71}BM$ (acceptor) through dispersion-type concave-convex interactions. Both materials were used in order to control the morphology of thin-film solar cells by self-assembly, yielding devices with power conversion efficiency (PCE) values of up to 2.6%.

In 2007, truxene-tetrathiafulvalene truxTTF emerged as an excellent supramolecular partner for recognition of C_{60} as well as C_{70}.[35-38] TruxTTF features a truxene core, which is decorated with three convalently linked dithiole units. The introduction of these dithiole rings in an all-*cis* configuration leads to a deviation from planarity of the truxene core, which adopts a bowl-shape geomety (figure 1).[37] Its relatively large concave aromatic surface allows for the self-assembly with fullerenes and fullerene derivatives, such as $PC_{61}BM$ and $PC_{71}BM$, with binding constants (K_a) in the range of 10^4 M^{-1} (Fig. S1, ESI). Recently, a new truxTTF-like derivative truxTTF-CO was synthetized.[38] TruxTTF-CO shows enhanced absorption properties in thin film, compared to truxTTF, while retaining the ability to bind with C_{60}, albeit with a significantly lower binding constant (K_a = 10^3 M^{-1}) with $PC_{61}BM$ and $PC_{71}BM$ (Fig. S2, ESI). TruxTTF-CO exhibits a push-pull structure where one dithiole ring is substituted for a weak electron-withdrawing ketone group. As a consequence, a new bathocromically shifted intramolecular charge-transfer band is observed in its electronic absorption spectrum, which expands to ca. 650 nm.

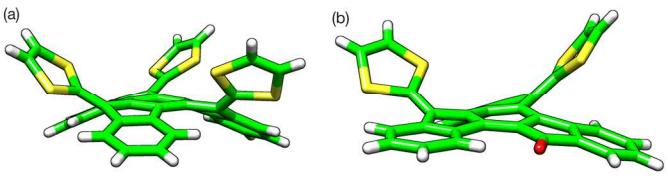

Figure 2. (a) X-Ray crystal structure of truxTTF[37] and (b) X-ray crystal structure of truxTTF-CO.[38] Carbon atoms are shown in green, sulfur in yellow and oxygen in red.

These characteristics make truxTTF and truxTTF-CO ideal candidates to investigate the relative importance of concave-convex interactions on the morphology and efficiency of OSCs. When using an electron acceptor with limited absorption properties, such as $PC_{61}BM$, morphology is a very important parameter to control. The stronger interactions (π-π, charge transfer and van der Waals interactions) between the concave face of the truxTTF and the convex face of the $PC_{61}BM$ could eventually lead to better self-organization of the photoactive layer (figure 2). These interactions between the donor and the acceptor are even stronger when using larger fullerene cages, such as $PC_{71}BM$, which could promote a more successful formation of the supramolecular complex and consequently well-defined donor-acceptor junctions.

Herein, we demonstrate that, at least for our particular systems, the molecular order induced by the concave-convex supramolecular interactions has a strong impact on the morphology and PCE values.

Results and discussion

Figure 3 shows optical absorption spectra of truxTTF and truxTTF-CO in dilute $CHCl_3$ solution and for spin-coated thin films. In solution, truxTTF-CO absorbs over a wider spectral range (300-655 nm) than truxTTF. TruxTTF-CO exhibits maximum absorption band (λ_{max}) at 400 nm and an intramolecular charge transfer (CT) band with low absorption at 550 nm, which is originated from electronic transitions from the dithiole rings to the carbonyl group.[33] On the other hand, truxTTF displays a sharper absorption peak centered at 449 nm, reflecting the lack of an intramolecular push-pull effect and higher loss of planarity. Moreover, both molecules exhibit similar absorption coefficient (ε) values (Fig S3, ESI). In the solid state, truxTTF and truxTTF-CO show broader absorptions, compared with those in solution, extending the absorption to 618 and 677 nm, for truxTTF and truxTTF-CO, respectively. The optical bands are estimated to be 2.00 eV and 1.83 eV for truxTTF and TruxTTF-CO respectively. Although not as pronounced as in solution, truxTTF-CO still absorbs over a wider spectral range in the thin films.

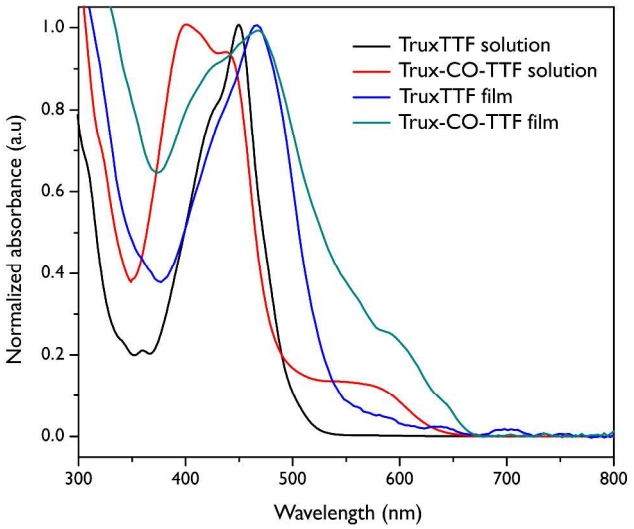

Figure 3. UV-vis absortion spectra of truxTTF and truxTTF-CO in diluted chloroform solution and in thin films.

The electrochemical properties of truxTTF and truxTTF-CO were analyzed by cyclic voltammetry (CV).[37,38] The highest occupied molecular orbital (HOMO) for truxTTF and truxTTF-CO were estimated from the oxidation onset potential to be -4.95 eV and -5.07 eV. The lowest unoccupied molecular orbital (LUMO) of truxTTF-CO was calculated from the onset reduction potential to be -3.4 eV. TruxTTF exhibits a LUMO of -2.95 eV, which was estimated from the optical band gap. The deeper HOMO level of truxTTF-CO should lead to an enhancement in the V_{oc} (figure 4b).

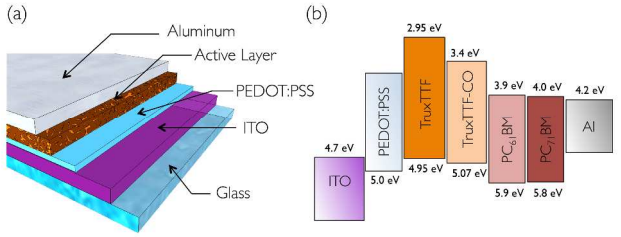

Figure 4. (a) Device structure of the conventional sandwich solar cells (ITO/PEDOT:PSS/Active layer/Al) and (b) energy-level diagram of the device.

To explore the properties of truxTTF and truxTTF-CO in photovoltaic devices, solar cells were fabricated using the conventional sandwich structure of ITO/PEDOT:PSS/Donor:Acceptor/Al or Ca/Al by using a varying weight ratio of the donor/$PC_{61}BM$ from 1:2 to 1:6 in a chlorobenzene:*ortho*-dichlorobenzene (o-DCB) (1:3) mixture. These experiments were performed under an ambient atmosphere employing AM 1.5G simulated illumination at an intensity of 100 mW cm^{-2}. The current density-voltage (*J-V)* characteristics and the external quantum efficiency (EQE) for the conventional device architecture ITO/PEDOT/active layer/Al are shown in figures 5a-d and the performance parameters are summarized in table 1 as a function of the weight ratios of donor:$PC_{61}BM$.

It is important to note that the D/A ratio strongly affects the V_{oc}, which can be attributed to a more effective supramolecular complexation (lower association constants were obtained using $PC_{61}BM$), but only slightly affects the fill factor (FF) and the short-circuit current density (J_{sc}). A photovoltaic device using truxTTF:$PC_{61}BM$ (1:2) w/w ratio yielded an average power conversion efficiency of 0.81%, with a V_{oc} of 0.63 V, a short-circuit current density (J_{sc}) of 4.28 mA cm^{-2} and a FF of 31.2%. Average values were taken from 10 devices. In addition, the overall efficiency and the V_{oc} decreased upon further increasing the $PC_{61}BM$ ratio, but the FF and the J_{sc} remained almost constant. On the other hand, the devices with a blend of truxTTF-CO:$PC_{61}BM$ (1:4) w/w ratio exhibited a PCE of 0.56%, with J_{sc} of 3.5 mA cm^{-2} and with significantly lower FF values than those observed for truxTTF, which is indicative of worse capacity to dissociate excitons and extract charge carriers and an unfavorable morphology. The bowl shaped contour of these small molecules donor favor a strong overlap with the acceptor, but such overlap also enables rapid charge recombination.

The external quantum efficiency (EQE) curves for devices based on different donor/acceptor (D/A) ratios, displayed in figure 5b, were investigated under monochromatic light. Both donor systems when blended with $PC_{61}BM$ exhibited a narrow spectral response, ranging from 300 to 700 nm. The devices containing truxTTF and $PC_{61}BM$ exhibited EQEs of 43% and 36% at 343 and 459 nm, respectively. The former corresponds to the photocurrent arising from the $PC_{61}BM$ and the latter corresponds to the contribution coming from the truxTTF. On the other hand, devices incorporating a blend of truxTTF-CO/$PC_{61}BM$ exhibited a broader but lower intensity photo-response with a shoulder at 594 nm, due to the broader light-harvesting abilities of the truxTTF-CO. The J_{sc} obtained from the *J-V* measurements and the integrated current densities from the EQEs are in good agreement, within ± 5%.

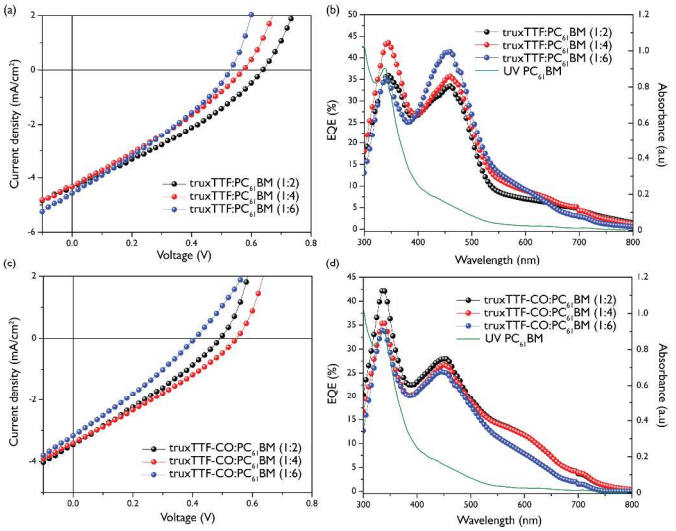

Figure 5. (a) Current density-voltage (*J-V*) curves of the blend truxTTF:$PC_{61}BM$, (b) EQE plots for the devices derived from truxTTF:$PC_{61}BM$ at different w/w ratio, (c) current density-voltage (*J-V*) curves of the blend truxTTF-CO:$PC_{61}BM$ and (d) EQE plots for the devices derived from truxTTF-CO:$PC_{61}BM$ at different w/w ratio.

To further explore the photovoltaic performances of truxTTF and truxTTF-CO donor compounds, solar cells were investigated with a different electron acceptor, namely $PC_{71}BM$ (Figure 6). It is known that the $PC_{61}BM$ absorbs over a narrower range and has lower extinction coefficient than $PC_{71}BM$ in the visible region. In thin film, $PC_{71}BM$ displays a broad absorption from 300 to 750 nm, whereas $PC_{61}BM$ has limited photo-response in the same region.

Photovoltaic devices incorporating truxTTF exhibited a higher power conversion efficiency for a blend ratio 1:6 w/w, with an V_{oc} of 0.6 V, a short-circuit current (J_{sc}) of 8.11 mA cm^{-2} and a FF of 33.1%, for an overall PCE average of 1.61% and a maximum PCE of 1.77%, which corresponds to an improvement of almost 100% with respect to those devices containing $PC_{61}BM$ as the electron acceptor (Table 2).

Table 1. Device performance parameters of the devices fabricated with truxTTF and truxTTF-CO blended with $PC_{61}BM$.

Active layer	V_{oc} (V)	J_{sc} (mA cm^{-2})	FF (%)	PCE [Highest](%)
truxTTF:$PC_{61}BM$ (1:6)	0.53±0.03	4.34±0.21	30.1±0.21	0.69±0.1 [0.72]
truxTTF:$PC_{61}BM$ (1:4)	0.57±0.01	4.42±0.17	30.2±0.19	0.76±0.1 [0.80]
truxTTF:$PC_{61}BM$ (1:2)	0.63±0.02	4.28±0.10	31.2±0.11	0.81±0.1 [0.92]
truxTTF-CO:$PC_{61}BM$ (1:6)	0.40±0.01	3.13±0.11	28.1±0.18	0.34±0.04 [0.36]
truxTTF-CO:$PC_{61}BM$ (1:4)	0.50±0.02	3.24±0.21	28.7±0.26	0.47±0.1 [0.56]
truxTTF-CO:$PC_{61}BM$ (1:2)	0.50±0.02	3.31±0.23	27.7±0.18	0.44±0.04 [0.47]

When the D/A ratio was adjusted from 1:6 to 1:2, the J_{sc} decreased from 8.11 to 4.87 mA cm^{-2} and the FF decreases from 33.1 to 30.8%. This experimental finding could be explained in terms of aggregation of truxTTF molecules when the amount of the donor increases, which results in the formation of larger domains of truxTTF, and therefore unsuccessful creation of the supramolecular complex.[33] In contrast, the best photovoltaic performance for truxTTF-CO was provided by the blend with a 1:4 w/w ratio (average PCE 1.06%, maximun of 1.19%), with a V_{oc} of 0.61 V, J_{sc} of 5.78 mA cm^{-2} and a FF of 30.2%. The V_{oc} values obtained are consistent with the difference between the donor HOMO and the LUMO of the $PC_{71}BM$ in both cases. Furthermore, the photovoltaic properties were investigated employing the best ratios for each donor molecule, with the device architecture of ITO/PEDOT:PSS/active layer/Ca/Al. The introduction of Ca as an electron transport layer (ETL) provides a higher built-in potential and a more efficient electron transport and collection process (increasing the FF). As expected, a remarkable improvement of 66 mV in the V_{oc} and more than 3% in the FF was achieved in a blend of truxTTF:$PC_{71}BM$, for a maximum efficiency of 1.77%. Surprisingly, no improvement was observed for the blend containing truxTTF-CO and $PC_{71}BM$ (1:4 w/w).

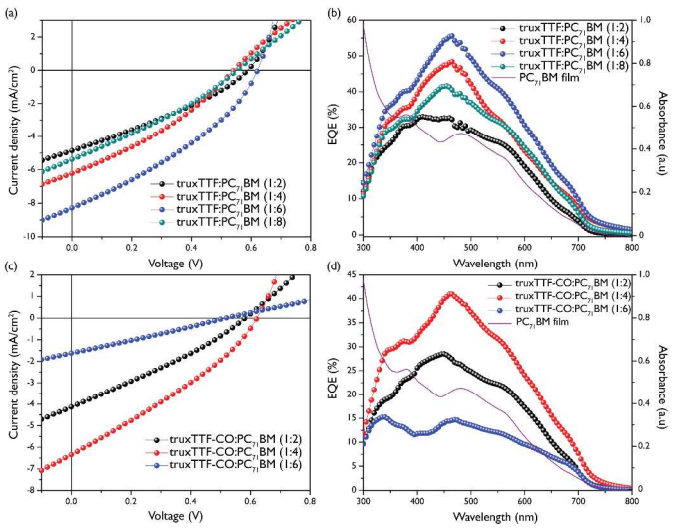

Figure 6. (a) Current density-voltage (*J-V*) curves of the blend truxTTF:$PC_{71}BM$, (b) EQE plots for the devices derived from truxTTF:$PC_{71}BM$ at different w/w ratio, (c) current density-voltage (*J-V*) curves of the blend truxTTF-CO:$PC_{71}BM$ and (d) EQE plots for the devices derived from truxTTF-CO:$PC_{71}BM$ at different w/w ratio.

Furthermore, in order to get further insights into the supramolecular assembly in thin film, 1,8-diiodooctane (DIO) was added. It was reported that the addition of DIO can hinder or inhibit the interactions between complementary faces of the donor and the acceptor.[33] As expected, the PCE for truxTTF:$PC_{71}BM$ (1:6) w/w and truxTTF-CO:$PC_{71}BM$ (1:4) w/w decreased when the DIO was present (Fig. S4 and S5, ESI).

It is important to emphasize that the FF was higher when truxTTF was used as electron donor. The FF is known to depend heavily on morphology/charge-recombination[39-42] and, in our case, truxTTF and $PC_{71}BM$ blends lead to higher efficiencies when compared to truxTTF-CO.

Figure 6b and 6d show the external quantum efficiency (EQE) curves for those devices based on varying D/A ratios. Both spectra of donor units blended with $PC_{71}BM$ exhibited a broader spectral response than those with $PC_{61}BM$, ranging from 300 to 750 nm, whereas the mixture of truxTTF:$PC_{71}BM$ at 1:6 w/w ratio reached the highest value of EQE (55%) at 463 nm. When the donor ratio decreases to 1:4 or 1:6, the contribution to the EQE is mainly from $PC_{71}BM$, but when the ratio is increased to 1:2 the contribution of the donor is similar to the contribution of the $PC_{71}BM$. For the blend based on truxTTF:$PC_{71}BM$ (1:6 w/w), the higher experimental J_{sc} values were 8.31 mA cm^{-2} whereas the estimated value of J_{sc} from the EQE measurements was 8.29 mA cm^{-2}. The corresponding devices containing truxTTF-CO:$PC_{71}BM$ displayed a lower EQE (41% at 460 nm for 1:4 ratio).

Table 2. Device performance parameters of the devices fabricated with truxTTF and truxTTF-CO blended with $PC_{71}BM$.

Active layer	V_{oc} (V)	J_{sc} (mA cm^{-2})	FF (%)	PCE [Highest](%)
truxTTF:$PC_{71}BM$ (1:8)	0.55±0.01	4.81±0.37	29.8±0.17	0.80±0.1 [0.89]
truxTTF:$PC_{71}BM$ (1:6)	0.60±0.03	8.11±0.22	33.1±0.28	1.61±0.1 [1.77]
truxTTF:$PC_{71}BM$ (1:4)	0.53±0.01	6.38±0.12	31.9±0.24	1.07±0.1 [1.15]
truxTTF:$PC_{71}BM$ (1:2)	0.58±0.02	4.87±0.10	30.8±0.11	0.83±0.1 [0.88]
truxTTF-CO: $PC_{71}BM$ (1:6)	0.51±0.01	1.49±0.14	26.3±0.15	0.2±0.02 [0.22]
truxTTF-CO: $PC_{71}BM$ (1:4)	0.61±0.02	5.78±0.31	30.2±0.22	1.06±0.1 [1.19]
truxTTF-CO: $PC_{71}BM$ (1:2)	0.56±0.02	3.82±0.25	29.0±0.21	0.62±0.04 [0.68]

The active layer morphologies incorporating truxTTF and truxTTF-CO, were characterized by atomic force microscopy (AFM) in tapping mode, using the best composition for each device, as shown in Figure 7. The images reveal that truxTTF presents a more favourable morphology when compared to that of truxTTF-CO.

The surface topographies of truxTTF:$PC_{61}BM$ (1:6) and truxTTF:$PC_{71}BM$ (1:6) blend films exhibit rather uniform nanometer-sized features with a root-mean-square roughness (rms) value of 0.33 nm and 0.31 nm, respectively. On the other hand, blends containing truxTTF-CO with $PC_{61}BM$ and $PC_{71}BM$ display slightly coarser topographies, with higher rms values of 0.47 nm and 0.43 nm, respectively. In addition, the truxTTF:$PC_{71}BM$ reveals the formation of slightly larger and better defined morphological features (10-50 nm), measured from cross-sectional profiles (Fig. S6, ESI), which is beneficial for exciton dissociation and charge transport.[43,44]

These experimental findings could be accounted for by the better miscibility of truxTTF with $PC_{71}BM$ which eventually results in an enhance device performance.

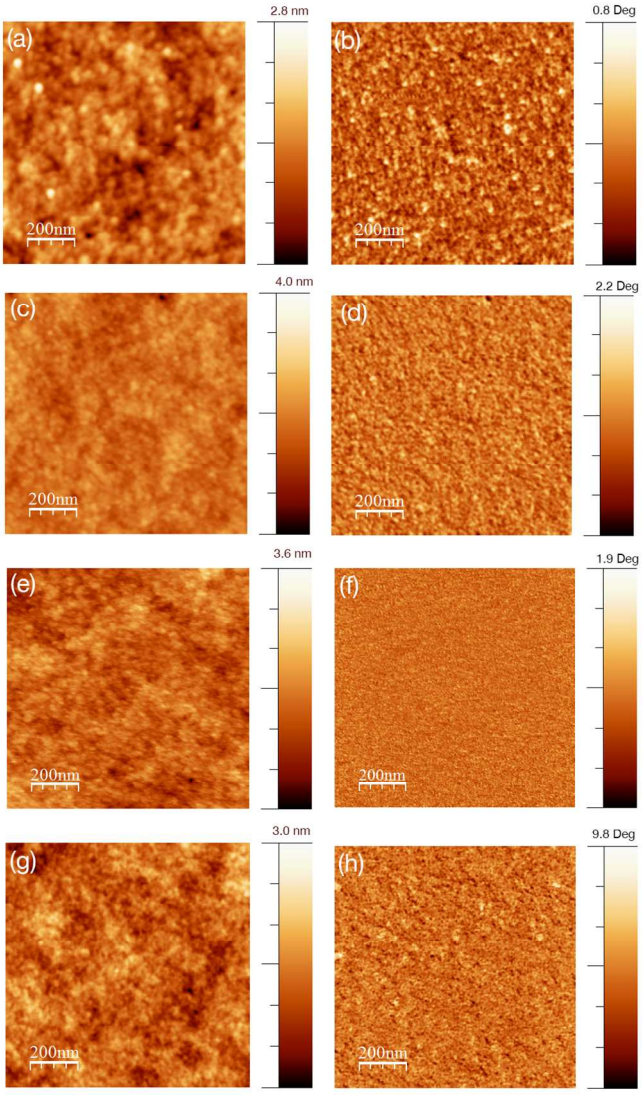

Figure 7. Tapping mode AFM height and phase images (1 µm x 1µm) of blends films spin-coated from chlorobenzene:o-DCB of (a and b) truxTTF:$PC_{61}BM$ (1:6), (c and d) truxTTF:$PC_{71}BM$ (1:6), (e and f) truxTTF-CO:$PC_{61}BM$ (1:4) and (g and h) truxTTF-CO:$PC_{71}BM$ (1:4).

Conclusions

In conclusion, a less-explored supramolecular approach has been used for the preparation of small-molecule solar cells. The highest PCE based on a truxTTF:$PC_{71}BM$ (1:6) w/w ratio was 1.77%, while incorporating truxTTF-CO yielded 1.19%. Although, both of them possess similar bowl-shape geometries that allow the formation of supramolecular complexes when blended with $PC_{61}BM$ or $PC_{71}BM$, they show different binding constants with fullerenes and also different optical properties. Despite the broader absorption and the deeper HOMO of truxTTF-CO, the stronger non-convalent interactions between the concave shape of the electron donating truxTTF and the convex surface of the fullerene derivatives lead to higher J_{sc} and FF, probably as a result of the more favorable morphology of the blends.

Acknowledgements

L. E. thanks the Robert A. Welch Foundation for an endowed chair, grant #AH-0033, the US National Science Foundation, grant DMR-1205302 (PREM Program) and the Air Force Office of Scientific Research (grants FA9550-12-1-0053 and FA9550-12-1-0468) for the generous financial support. We are thankful to A. Soubrié (Centro de Microscopía y Citometría, UCM) for AFM imaging. M.G. acknowledges the Spanish Ministry of Education, Culture and Sport (MECD) for a FPU studentship. Financial support by the Ministerio de Economia y Competitividad (MINECO) of Spain (project CTQ2011-24652), the CAM (FOTOCARBON project S2013/MIT-2841), PRI-PRIBUS (2011-1067) and the European Research Council (ERC-320441-Chirallcarbon) is acknowledged. N. M. thanks to Alexander von Humboldt Foundation.

Notes and references

[a] Department of Chemistry, University of Texas at El Paso, 79968, El Paso, Texas (USA).
[b] IMDEA-nanociencia, C/Faraday 9, Ciudad Universitaria de Cantoblanco, 28049 Madrid (Spain)
[c] Departamento de Química Orgánica, Fac. C.C. Químicas, Universidad Complutense de Madrid, Av. Complutense s/n, 28040 Madrid (Spain)
Homepage: http://www.ucm.es/info/fullerene/

Electronic Supplementary Information (ESI) available: [details of any supplementary information available should be included here]. See DOI: 10.1039/b000000x/

1. C. J. Brabec, S. Gowrisanker, J. J. M. Halls, D. Laird, S. Jia, and S. P. Williams, *Adv. Mater.*, 2010, **22**, 3839–3856.
2. J.-T. Chen and C.-S. Hsu, *Polym. Chem.*, 2011, **2**, 2707-2722.
3. A. Mishra and P. Bauerle, *Angew. Chem., Int. Ed.*, 2012, **51**, 2020–2067.
4. Y. Lin, Y. Li, and X. Zhan, *Chem. Soc. Rev.*, 2012, **41**, 4245-4272.
5. B. C. Thompson and J. M. J. Frechet, *Angew. Chem., Int. Ed.*, 2008, **47**, 58–77.
6. A. J. Moulé and K. Meerholz, *Adv. Funct. Mater.*, 2009, **19**, 3028–3036.
7. G. Dennler, M. C. Scharber, and C. J. Brabec, *Adv. Mater.*, 2009, **21**, 1323–1338.
8. F. Yang, M. Shtein, and S. R. Forrest, *Nat. Mater.*, 2004, **4**, 37–41.
9. J. Peet, M. L. Senatore, A. J. Heeger, and G. C. Bazan , *Adv. Mater.*, 2009, **21**, 1521–1527.
10. J. L. Delgado, P.-A. Bouit, S. Filippone, M. A. Herranz, N. Martín, *Chem. Commun.*, 2010, **46**, 4853-4865.
11. Y. Huang, E. J. Kramer, A. J. Heeger, and G. C. Bazan, *Chem. Rev.*, 2014, **114**, 7006–7043.
12. J. Peet, J. Y. Kim, N. E. Coates, W. L. Ma, D. Moses, A. J. Heeger, and G. C. Bazan, *Nat. Mater.*, 2007, **6**, 497–500.
13. S. J. Lou, J. M. Szarko, T. Xu, L. Yu, T. J. Marks, and L. X. Chen, *J. Am. Chem. Soc.*, 2011, **133**, 20661–20663.
14. J. K. Lee, W. L. Ma, C. J. Brabec, J. Yuen, J. S. Moon, J. Y. Kim, K. Lee, C. Bazan Guillermo, and A. J. Heeger, *J. Am. Chem. Soc.*, 2008, **130**, 3619–3623.
15. G. Li, V. Shrotriya, J. Huang, Y. Yao, T. Moriarty, K. Emery, and Y. Yang, *Nat. Mater.*, 2005, **4**, 864–868.
16. G. Li, Y. Yao, H. Yang, V. Shrotriya, G. Yang, and Y. Yang, *Adv. Funct. Mater.*, 2007, **17**, 1636–1644.
17. W. Ma, C. Yang, X. Gong, K. Lee, and A. J. Heeger, *Adv. Funct. Mater.*, 2005, **15**, 1617–1622.
18. M. Campoy-Quiles, T. Ferenczi, T. Agostinelli, P. G. Etchegoin, Y. Kim, T. D. Anthopoulos, P. N. Stavrinou, D. D. C. Bradley, and J. Nelson, *Nat. Mater.*, 2008, **7**, 158–164.
19. S. Miller, G. Fanchini, Y.-Y. Lin, C. Li, C.-W. Chen, W.-F. Su, and M. Chhowalla, *J. Mater. Chem.*, 2008, **18**, 306-312.
20. G. Wei, S. Wang, K. Sun, M. E. Thompson, and S. R. Forrest, *Adv. Energy Mater.*, 2011, **1**, 184–187.
21. G. Wei, R. R. Lunt, K. Sun, S. Wang, M. E. Thompson, and S. R. Forrest, *Nano Lett.*, 2010, **10**, 3555–3559.
22. T. A. Bull, L. S. C. Pingree, S. A. Jenekhe, D. S. Ginger, and C. K. Luscombe, *ACS Nano*, 2009, **3**, 627–636.
23. R. D. Kennedy, A. L. Ayzner, D. D. Wanger, C. T. Day, M. Halim, S. I. Khan, S. H. Tolbert, B. J. Schwartz, and Y. Rubin, *J. Am. Chem. Soc.*, 2008, **130**, 17290–17292.
24. C. J. Tassone, A. L. Ayzner, R. D. Kennedy, M. Halim, M. So, Y. Rubin, S. H. Tolbert, and B. J. Schwartz, *J. Phys. Chem. C*, 2011, **115**, 22563–22571.
25. N. C. Cates, R. Gysel, Z. Beiley, C. E. Miller, M. F. Toney, M. Heeney, I. McCulloch, and M. D. McGehee, *Nano Lett.*, 2009, **9**, 4153–4157.
26. C. Bruner, N. C. Miller, M. D. McGehee, and R. H. Dauskardt, *Adv. Funct. Mater.*, 2013, **23**, 2863-2871.
27. N. C. Miller, S. Sweetnam, E. T. Hoke, R. Gysel, C. E. Miller, J. A. Bartelt, X. Xie, M. F. Toney, and M. D. McGehee, *Nano Lett.*, 2012, **12**, 1566–1570.
28. K. H. Lam, T. R. B. Foong, Z. E. Ooi, J. Zhang, A. C. Grimsdale, and Y. M. Lam, *ACS Appl. Mater. Interfaces*, 2013, **5**, 13265–13274.
29. B. M. Schulze, N. T. Shewmon, J. Zhang, D. L. Watkins, J. P. Mudrick, W. Cao, R. Bou Zerdan, A. J. Quartararo, I. Ghiviriga, J. Xue, and R. K. Castellano, *J. Mater. Chem. A*, 2014, **2**, 1541-1549.
30. A. Ruiz-Carretero, T. Aytun, C. J. Bruns, C. J. Newcomb, W.-W. Tsai, and S. I. Stupp, *J. Mater. Chem. A*, 2013, **1**, 11674-11681.
31. C.-H. Huang, N. D. McClenaghan, A. Kuhn, J. W. Hofstraat, and D. M. Bassani, *Org. Lett.*, 2005, **7**, 3409–3412.
32. S. J. Kang, J. B. Kim, C.-Y. Chiu, S. Ahn, T. Schiros, S. S. Lee, K. G. Yager, M. F. Toney, Y.-L. Loo, and C. Nuckolls, *Angew. Chem., Int. Ed.*, 2012, **51**, 8594–8597.
33. S. J. Kang, S. Ahn, J. B. Kim, C. Schenck, A. M. Hiszpanski, S. Oh, T. Schiros, Y.-L. Loo, and C. Nuckolls, *J. Am. Chem. Soc.*, 2013, **135**, 2207–2212.
34. S. Xiao, S. J. Kang, Y. Wu, S. Ahn, J. B. Kim, Y.-L. Loo, T. Siegrist, M. L. Steigerwald, H. Li, and C. Nuckolls, *Chem. Sci.*, 2013, **4**, 2018-2023.
35. E. M. Pérez, N. Martín, *Chem. Soc. Rev.*, 2008, **37**, 1512–1519.
36. M. Gallego, J. Calbo, J. Aragó, R. M. K. Calderon, F. H. Liquido, A. Iwamoto, A. K. Greene, E. A. Jackson, E. M. Pérez, E. Ortí, D. M.

Guldi, L. T. Scott, N. Martín, *Angew. Chem. Int. Ed.* 2014, **53**, 2170 –2175
37. E. M. Perez, M. Sierra, L. Sánchez, M. R. Torres, R. Viruela, P. M. Viruela, E. Orti, and N. Martín, *Angew. Chem., Int. Ed.*, 2007, **46**, 1847–1851.
38. H. Isla, B. Grimm, E. M. Perez, M. Rosario Torres, M. Angeles Herranz, R. Viruela, J. Aragó, E. Orti, D. M Guldi, and N. Martín, *Chem. Sci.*, 2012, **3**, 498-508.
39. V. D. Mihailetchi, H. X. Xie, B. de Boer, L. J. A. Koster, and P. W. M. Blom, *Adv. Funct. Mater.*, 2006, **16**, 699–708.
40. B. Qi and J. Wang, *Phys. Chem. Chem. Phys.*, 2013, **15**, 8972-8982.
41. D. Gupta, S. Mukhopadhyay, and K. S. Narayan, *Sol. Energy Mater. Sol. Cells*, 2010, **94**, 1309–1313.
42. G. Li, R. Zhu, and Y. Yang, Nat. Photonics, 2012, **6**, 153–161.
43. C. R. McNeill, S. Westenhoff, C. Groves, R. H. Friend, and N. C. Greenham, *J. Phys. Chem. C*, 2007, **111**, 19153–19160.
44. Y. Yao, J. Hou, Z. Xu, G. Li, and Y. Yang, *Adv. Funct. Mater.*, 2008, **18**, 1783–1789.